



# Highly ordered Zn-doped mesoporous silica: An efficient catalyst for transesterification reaction

Nabanita Pal, Manidipa Paul, Asim Bhaumik\*

Department of Materials Science, Indian Association for the Cultivation of Science, Jadavpur, Kolkata 700032, India

## ARTICLE INFO

### Article history:

Received 26 January 2011

Received in revised form

16 May 2011

Accepted 23 May 2011

Available online 30 May 2011

### Keywords:

Ordered mesoporous silica

Zn-loading

Transesterification

Surface area

Surface acidity

## ABSTRACT

Designing highly ordered material with nanoscale periodicity is of great significance in the field of solid state chemistry. Herein, we report the synthesis of highly ordered 2D-hexagonal mesoporous zinc-doped silica using a mixture of anionic and cationic surfactants under hydrothermal conditions. Powder XRD,  $N_2$  sorption, TEM analysis revealed highly ordered 2D-hexagonal arrangements of the pores with very good surface area ( $762 \text{ m}^2 \text{ g}^{-1}$ ) in this Zn-rich mesoporous material. Chemical analysis shows very high loading of zinc (ca. 12.0 wt%) in the material together with retention of hexagonal pore structure. Interestingly, high temperature calcination resulted into zinc silicate phase, unlike any ZnO phase, which otherwise is expected under heat treatments. High surface area together with Zn loading in this mesoporous material has been found useful for the catalytic activity of the materials in the acid-catalyzed transesterification reactions of various esters under mild liquid phase conditions.

© 2011 Elsevier Inc. All rights reserved.

## 1. Introduction

Doping of Zn in various inorganic framework structures is one of the frontier areas of research in solid state chemistry as the resulting materials find wide application in optoelectronics [1], sensing [2], biology [3], catalysis [4], photocatalysis [5] and so on. Zinc oxide nanostructures are extensively studied in the literature for its interesting photoconducting [6], electrical [7] and optical properties [8]. In addition, crucial role played by Zn(II) in pure ZnO and its mixed oxides in heterogeneous catalysis makes many organic reactions feasible. Industrial methanol synthesis [9], chemo-selective hydrogenation of aldehydes [10], transesterification reactions [11], etc. are the most common of them. Transesterification reaction of esters is an important organic transformation useful for synthesis of a large variety of esters, especially in the production of biodiesel and many synthetic materials [12,13]. This reaction may proceed in presence of either basic or acidic catalyst. ZnO and other zinc complexes have surface Lewis acidic property and thus catalyze few transesterification reactions [14]. However, Zn-doped ordered mesoporous material has not been synthesized and employed in the transesterification reactions.

Since its discovery, M41S family of ordered mesoporous materials [15,16] have attracted wide interest in the field of catalysis due to their exceptional surface area and tunable pores of

nanoscale dimensions. But pure silica materials like MCM-41 or SBA-15 found limited application in heterogeneous catalysis due to the absence of acidic or redox species in the materials. The substitution of Si atom by other active metal ions of similar atomic size could modify the structural properties of the resulting metal-doped silica and thus leads to great improvement in catalytic performances [17–19]. In this context incorporation of transition metal ions to the silica framework has been widely investigated in last few decades due to their application in eco-friendly, industrially important catalytic reactions [20–22]. Like other elements Zn metal incorporated silica materials show crucial role in heterogeneous catalysis. Previously, Silvestre-Albero et al. [4] reported Zn containing MCM-41 and studied its catalytic behavior. However, the amount of Zn loading in the siliceous framework was quite low and this could be attributed to its limited catalytic activity. Hence, synthesis of ordered mesoporous silica with high Zn content is quite challenging task, which is not reported till date. We have synthesized Zn-rich silica material via a simple co-condensation method of Zn(II) and silicate precursors in the presence of a mixture of surfactants CTAB and SDS. In this context it is pertinent to mention that the imperative role of tartaric acid in the synthesis of metallosilicate has been proved before [23,24]. We have used tartaric acid to increase the Zn loading in the silica framework and build a stable mesoporous Zn-doped matrix.

Furthermore, the stoichiometric compound zinc silicate ( $\text{Zn}_2\text{SiO}_4$ ) with  $\alpha$ -willemit structure is of significant importance for its various commercial applications [25]. A variety of methods have been reported related to the synthesis of  $\text{Zn}_2\text{SiO}_4$  nanostructure [26]. But to the best of our knowledge, no attempt has

\* Correspondence to: Department of Materials Science, Indian Association for the Cultivation of Science, 2A & B Raja S.C. Mullick Road, Jadavpur, Kolkata 700032, India. Fax: +91 33 2473 2805.

E-mail address: [msab@iacs.res.in](mailto:msab@iacs.res.in) (A. Bhaumik).

been made to obtain  $\alpha$ -willemitite  $Zn_2SiO_4$  nanostructured material via Zn-doped ordered mesoporous silica. Our present study deals with the conversion of amorphous Zn containing silica material to crystalline zinc silicate on high temperature calcination. Herein, we report the synthesis of Zn-rich highly ordered mesoporous silica, its detailed characterizations and catalytic application in the transesterification reaction.

## 2. Experimental section

### 2.1. Materials used

Tetraethyl orthosilicate (TEOS, Sigma-Aldrich) and zn(II) chloride (E-Merck) were used as silica and zinc sources, respectively. Surfactants cetyltrimethylammonium bromide (CTAB, Loba Chemie) and sodium dodecylsulphate (SDS, Loba Chemie) were used as templates. DL-Tartaric acid (TA, E-Merck) was used to stabilize Zn(II) through complex formation and thus to have better interaction with the silicate species during hydrothermal synthesis. For pH adjustment tetramethylammonium hydroxide (TMAOH, 25% aqueous solution, Sigma-Aldrich) solution was used.

### 2.2. Procedure

We prepared three samples by co-condensation method with different Zn:Si molar ratios varying from (2–10):50. In a typical synthesis, SDS (0.47 g) was mixed with tartaric acid (TA, 1.31 g) in a plastic beaker containing about 60 g distilled water. After few minutes CTAB (3.00 g) was added to the above solution under vigorous stirring at room temperature. Immediately the mixture became viscous and this was kept under stirring for about 30 min. Next, TEOS (3.5 g) was added to this suspension under continuous stirring. The suspension was vigorously stirred for about 2–3 h, which enhances the miscibility of the organic phase with aqueous phase along with the hydrolysis of the silicate species. Then 0.50 g  $ZnCl_2$  (for samples ZS-5/5A) dissolved in 2 g  $H_2O$  was added slowly to the resulting mixture followed by constant stirring for another 4 h. After that TMAOH solution was added dropwise to this mixture and a heavy white precipitate appeared gradually. The pH was maintained strictly to *ca.* 11.0. The resultant mixture was aged overnight under stirring at room temperature and finally transferred to a polypropylene bottle for hydrothermal treatment at 353 K during 72 h. Finally the solid product was recovered by filtration, washed thoroughly with water so that the surface of the sample was totally free from adhered loosely bound Zn(II) ions. White product was dried at room temperature and calcined at 703 K temperature to take out the organic templates from the material. Calcined sample was designated as ZS-5. For other two batches the resulting calcined powder samples were synthesized following the same procedure and named as ZS-10 (Si/Zn molar ratio=10:1) and ZS-25 (Si/Zn molar ratio=25:1). The molar ratios of various constituents for all the above samples were (2–10)  $ZnCl_2$ :50.0 TEOS:25.0 CTAB:5.0 SDS:50.0 TA:9860  $H_2O$ . The sample

ZS-5 was further heated at temperature 1173 K for 2 h to enhance the crystallinity of the pore-wall.

### 2.3. Characterizations

Powder X-ray diffraction (XRD) patterns of the materials were recorded on a Bruker AXS D-8 Advance diffractometer operated at 40 kV voltage and 40 mA current and calibrated with a standard silicon sample, using Ni-filtered  $CuK\alpha$  ( $\lambda=0.15406$  nm) radiation. Nitrogen and adsorption/desorption isotherms were obtained using a Beckmann Coulter SA 3100 surface area analyzer at 77 K. Prior to the measurement, all the samples were degassed at 453 K. JEOL JEM 6700F field emission scanning electron microscope (FE SEM) with an energy dispersive X-ray spectroscopic (EDS) attachment was used to record the morphology of the sample and its surface chemical composition. Transmission electron microscopy (TEM) images were recorded in a JEOL JEM 2010 transmission electron microscope. Fourier transform infrared (FT IR) spectra of these samples were recorded on KBr pellets by using a Shimadzu FT IR 8300 spectrophotometer. Thermogravimetry (TG) and differential thermal analysis (DTA) were carried out on a TA instrument Q600 DSC/TGA thermal analyzer. UV-visible diffuse reflectance spectra were recorded by using a Shimadzu UV 2401PC spectrophotometer with an integrating sphere attachment and  $BaSO_4$  pellet was used as background standard. The Zn content of the samples was measured using Shimadzu AA-6300 atomic absorption spectrophotometer (AAS) by dissolving the solid powder in aqueous solution containing minimum amount HF/HCl.

### 2.4. Procedure for the catalytic transesterification reactions

The transesterification reactions of different ethyl esters were carried out in a 50 ml capacity round bottom flask fitted with a water condenser and placed in a temperature controlled oil bath under constant stirring at a fixed temperature. Methanol, 1-butanol, 2-propanol or benzyl alcohols (all procured from Merck, India) were used as transesterification reagents and required amount of solid catalyst was added. The reactions were carried out with or without solvent. At different interval of time reaction mixture was monitored by thin layer chromatography (TLC) using 10% ethyl acetate-pet ether solution. After the reaction was completed, solid catalyst was filtered and the alcohol was evaporated by using a rotary evaporator. The products were identified by  $^1H$  NMR spectroscopy and percentage of conversion was measured by capillary Gas Chromatography (GC, Agilent 4890D, with FID detector).

## 3. Results and discussions

### 3.1. Synthesis conditions

The physico-chemical characterizations of all zinc-doped mesoporous silica materials are enlisted in Table 1. In order to synthesize 2D hexagonally ordered mesophase we have employed mixture of surfactants, cationic CTAB and anionic SDS in the

**Table 1**  
Physico-chemical properties of all mesoporous zinc-doped silica samples.

Sample name	Zn:Si ratio synthesis mixture	Zn:Si ratio product		BET surface area ( $m^2 g^{-1}$ )	Pore volume ( $cc g^{-1}$ )	Pore diameter (nm)	d spacing XRD (nm)	Wall thickness (nm)
		EDS	AAS					
ZS-5	1:5	1:7	1:8	762	0.87	2.98	3.68	0.70
ZS-10	1:10	1:10	1:9	765	0.87	3.05	3.72	0.67
ZS-25	1:25	1:15	1:14	799	0.90	2.58	3.54	0.96

synthesis mixtures in the presence of tartaric acid. The Zn:Si ratio calculated from AAS analysis almost matches with that obtained from surface analysis through EDS technique (Table 1), suggesting uniform distribution of Zn/Si at the surface and bulk. Self-assembly of both anionic and cationic templates is employed for the high loading of Zn in the mesophase. Beside this the presence of tartaric acid (complexing agent for Zn(II)) is also required for the *in situ* doping of Zn metal in the silica matrix under hydrothermal condition at a suitable temperature. Usually, increase of the zinc loading in the mesoporous silica system results a decrease in specific surface area and the ordering of the mesophase [5]. But in our ZS-5 sample, highly ordered mesophase has been retained at higher Zn loading in the synthesis mixture. The reason is the use of tartaric acid, which assists the incorporation of more Zn centers in the internal surface of the silica matrix forming stable complex with Zn(II) in aqueous medium and mixed surfactants favor the formation of highly ordered mesophase under the reaction conditions [23,24]. When the hydrothermal synthesis is carried out at an elevated temperature (beyond the optimum 353 K) poorly ordered mesophase is formed. Thus, we have chosen the lowest possible synthesis temperature for the hydrothermal treatment, which resulted in the material with greater surface area, together with highly ordered mesophase and high Zn loading. All samples are prepared under optimum temperature 353 K.

### 3.2. Nanostructure and mesophase

Small angle powder XRD patterns of the as-synthesized and calcined Zn-doped mesoporous silica samples with highest Zn content (ZS-5) are shown in Fig. 1. The peaks at  $2\theta$  ca.  $2.25^\circ$ ,  $3.98^\circ$ ,  $4.44^\circ$ ,  $6.03^\circ$ , which could be attributed to the characteristic peaks for 100, 110, 200 and 210 planes for the 2D-hexagonal mesophase [27,28] are clearly seen in XRD pattern of as-synthesized ZS-5A material. Presence of these diffraction peaks indicate that the sample possess 2D-hexagonal mesophase with highly ordered structure and ordered phase is retained after calcination. Other mesoporous samples (ZS-10, ZS-25) also exhibit similar XRD patterns, though the intensity of the peaks increases with increasing Si/Zn ratio. Respective small angle XRD patterns of all the calcined ZS-5/10/25

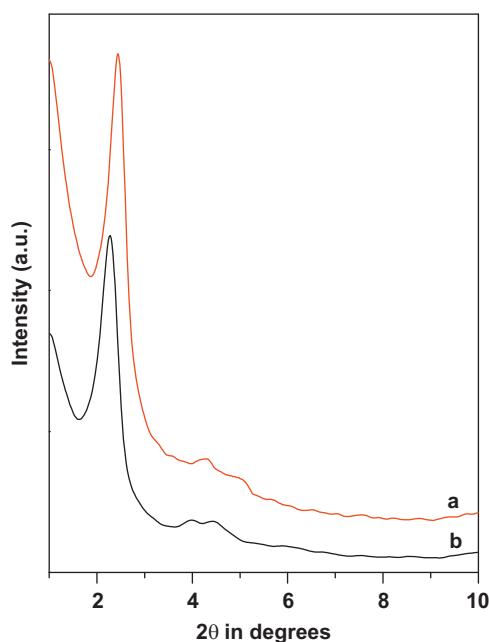


Fig. 1. Small angle powder XRD patterns of ZS-5 (a) and ZS-5A (b).

samples are shown in Fig. 2. As seen from this figure that intensity of 210 plane of this pattern decreases with an increase in Zn loading, suggesting a decrease in long range ordering of the mesophases in that order. In Fig. 3 wide angle powder XRD pattern of the calcined sample (further heated at 1173 K for 2 h) shows a good crystalline feature. This XRD pattern matches well with the  $\alpha$ -willemitite  $\text{Zn}_2\text{SiO}_4$  phase (JCPDS file no. 37-1485). The peak at  $36.2^\circ$  (marked with asterisk) is the only discrepancy observed and this could be attributed to minor impurity  $\text{SiO}_2$  phase ( $\alpha$ -cristobalite, JCPDS card 11-695) [29]. Thus, this experimental observation suggests that zinc is present in the mesoporous framework and the Zn-doped silica matrix changes to  $\text{Zn}_2\text{SiO}_4$  phase after high temperature treatment. The average crystallite size of this sample is 19.7 nm as calculated using the Scherrer equation [30].

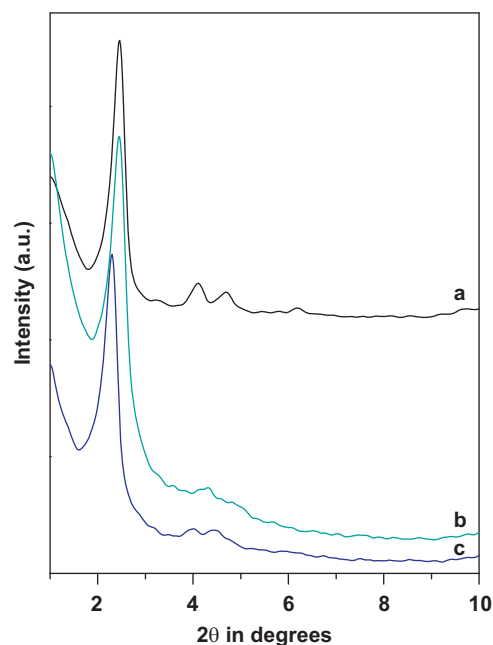


Fig. 2. Small angle XRD patterns of ZS samples: ZS-25 (a), ZS-10 (b) and ZS-5 (c).

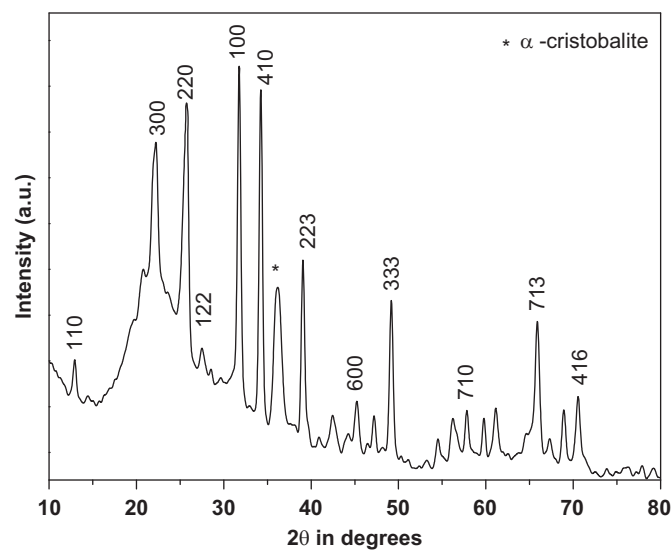


Fig. 3. Wide angle powder XRD pattern of mesoporous ZS-5 heated at temperature 1173 K. Impurity silica peak has been marked by asterisk.

### 3.3. Porosity and surface area

Information about surface area and pore size could be obtained from  $N_2$ -sorption measurement of the template-free sample at 77 K. In Fig. 4 the adsorption–desorption isotherms of calcined ZS-5 are shown. A typical type IV isotherm with hysteresis at higher  $P/P_0$  is observed here. Capillary condensation due to the steep rise of the isotherm, characteristic of other mesoporous materials is occurred here also [15,27,28]. The BET surface area and average pore volumes of the ZS-5, 10 and 25 samples are 762, 765 and 799  $m^2 g^{-1}$ , and 0.87, 0.87 and 0.90  $cm^3 g^{-1}$ , respectively (Table 1). The change in the surface area of different samples could be attributed to relative ordering of the mesophases. The narrow pore size distribution with maxima near 2.98 nm is estimated using NLDFT method [31], as seen in the inset of Fig. 4. Thus the average pore width of these mesoporous Zn-doped silica material is ca. 3.0 nm. On calcination at 1173 K this sample transforms into  $\alpha$ -willemite  $Zn_2SiO_4$  together with type IV isotherm for mesoporous nature and desorption hysteresis loop (not shown). However, the BET surface area has been decreased considerably to ca. 60  $m^2 g^{-1}$ . This could be attributed to partial collapse of the mesostructure at high temperature heat treatment (1173 K).

### 3.4. Electron microscopic analysis

A detail qualitative examination of the porous nanostructure in Zn-doped silica material is attained from the TEM image analysis. Fig. 5 represents the TEM image of as-synthesized ZS-25A sample. As seen from this image that hexagonal arrangement of the pores with different contrast than that of the pore wall is well observed throughout the specimen. The Fast Fourier Transform (FFT) pattern (inset of Fig. 5) further proves this hexagonal ordering of the pore channels in Zn-doped mesoporous silica sample. The TEM image of calcined ZS-5 sample is shown in Fig. 6. As seen from the figure that hexagonal arrangement of

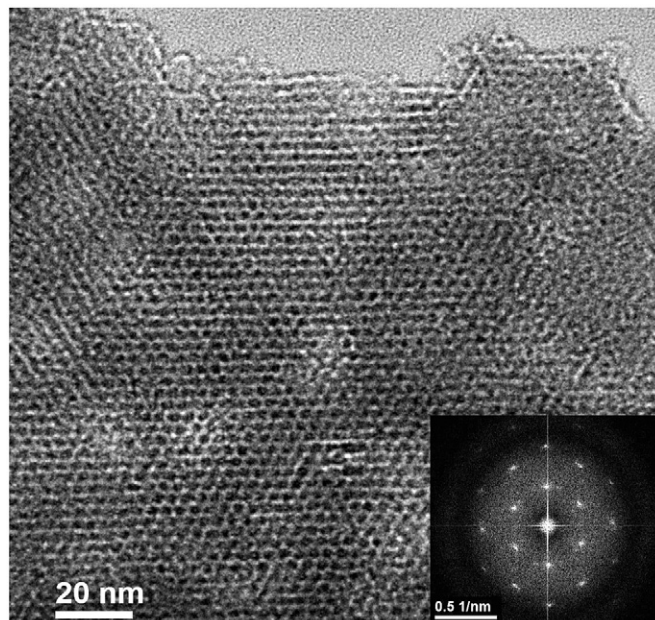


Fig. 5. TEM image of as-synthesized ZS-25 sample with the corresponding FFT pattern (inset).

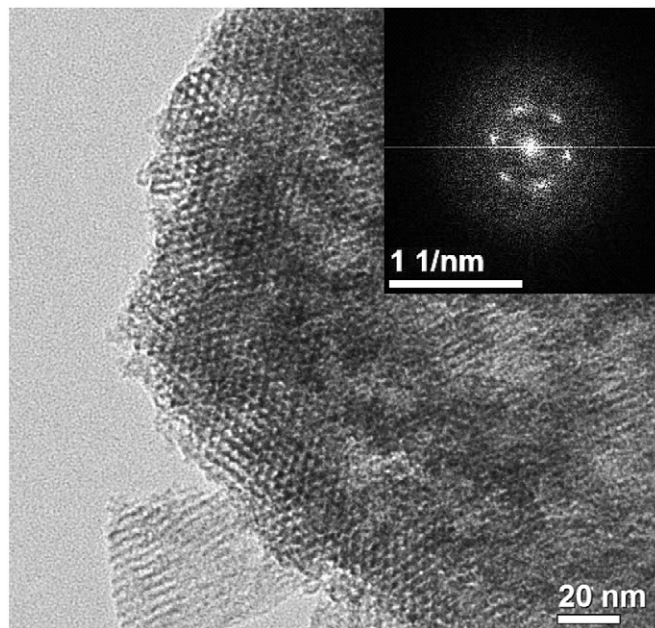


Fig. 6. TEM image of ZS-5 sample with the corresponding FFT pattern (inset).

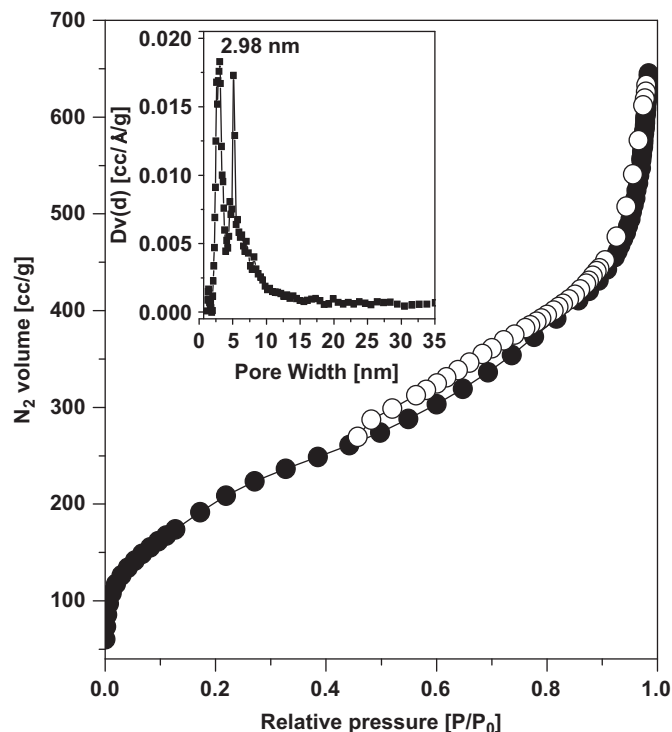


Fig. 4.  $N_2$  adsorption (●)–desorption (○) isotherms of mesoporous ZS-5 measured at 77 K. Pore size distribution is shown in inset.

pores are retained in this calcined sample. Corresponding FFT pattern (shown in inset) also suggests the hexagonal array of pore channels. Textural property and particle size of the Zn-doped mesoporous silica materials are explored from the SEM images. In Fig. 7 a representative SEM image of the ZS-5 sample is shown. Uniform distribution of small spherical particles of dimension 70–80 nm size is observed throughout the image. ZS-10/25 samples show almost similar morphological features in their respective SEM image. EDS spectrum of the corresponding ZS-5 sample is shown in Fig. 8. The strong signals for Zn, Si and O elements in the materials are observed. Absence of any peak for C proves complete removal of the organic templates. EDS data (Table 1) indicates that Zn/Si ratio is relatively lower than that

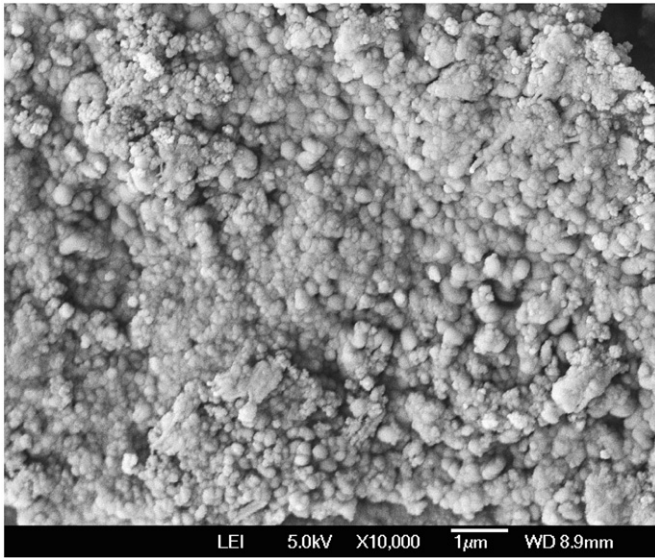


Fig. 7. FE SEM image of mesoporous ZS-5 sample.

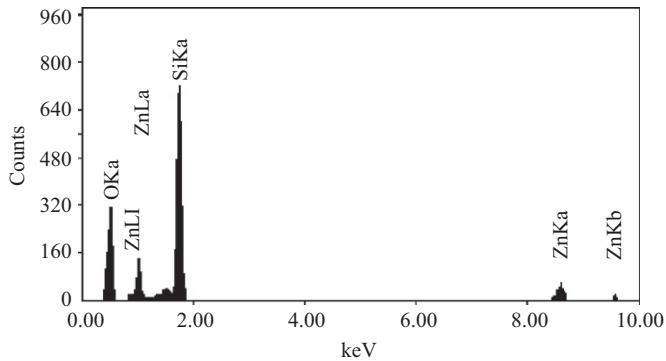


Fig. 8. EDS profile of sample ZS-5.

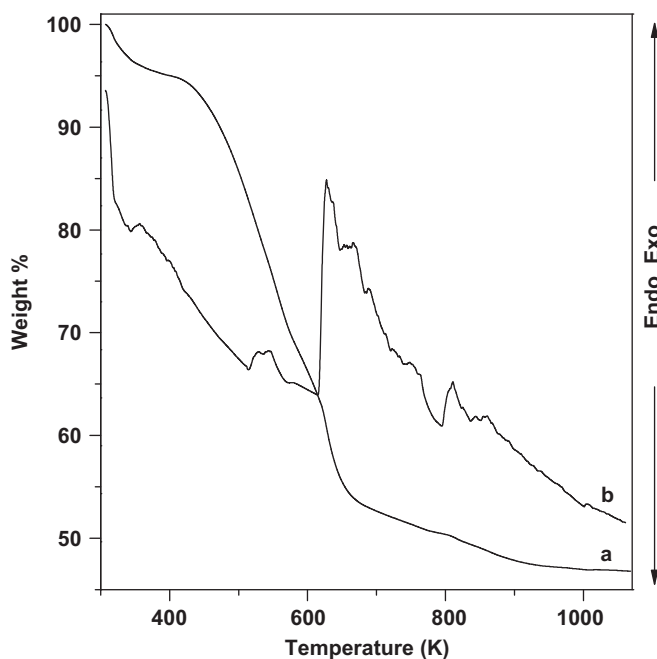


Fig. 9. TGA (a) and DTA (b) curves of as-synthesized ZS-5A sample.

of the synthesis mixture, suggesting Zn-rich mesophases in ZS-5/10/25 samples.

### 3.5. Thermal analysis

Thermogravimetric analysis provides useful information regarding the thermal stability of nanostructured materials. In Fig. 9 the TGA (a) and DTA (b) curves of the as-synthesized sample ZS-5A are shown. As seen from the TGA curve (a), that small weight loss of ca. 5.0% occurred until 400 K, which is due to the release of surface adsorbed water. Then a considerably large

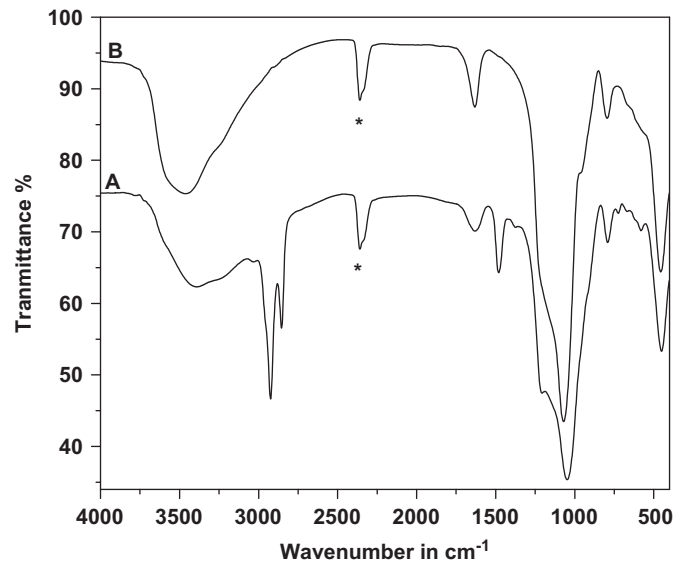


Fig. 10. FT IR spectra of as-synthesized ZS-5A (A) and mesoporous ZS-5 (B) samples. The peak marked with asterisk is for CO<sub>2</sub>.

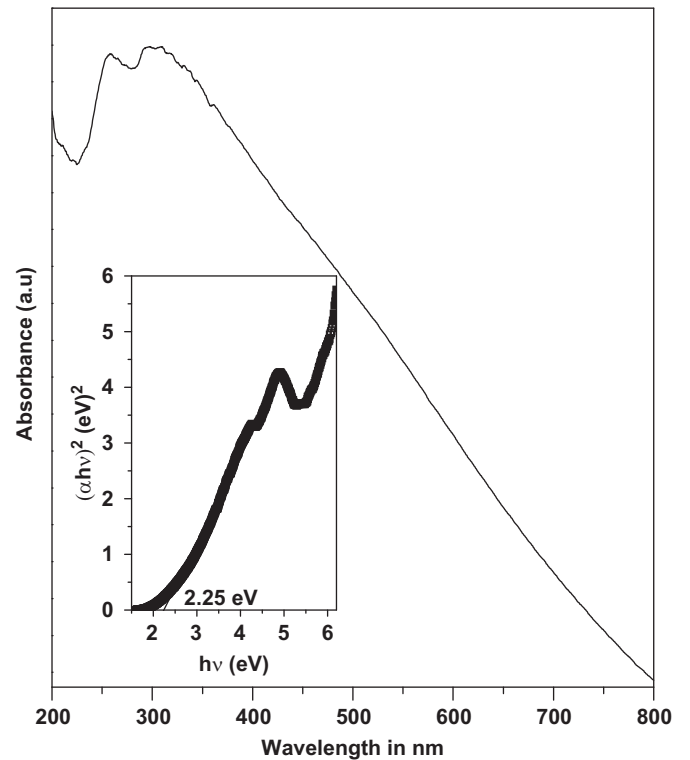
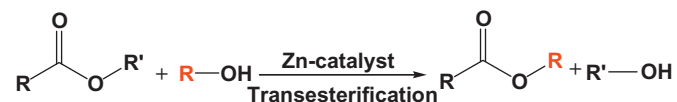


Fig. 11. UV-visible diffuse reflectance spectrum of mesoporous ZS-5 sample. Band gap is shown in inset.

weight loss is occurred until 690 K. This could be attributed to the burning of template molecules, which consist about 40% of the total as-synthesized material. The DTA curve shows a strong exothermic peak confirming the decomposition of the template

molecules here. After 700 K as the temperature further increases the template-free Zn-doped silica matrix changes to zinc silicate framework, which corresponds to *ca.* 48% of the total mass. The respective DTA curve shows a small exothermic peak in support to this phase change.

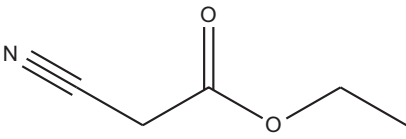
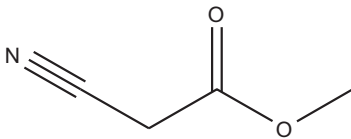
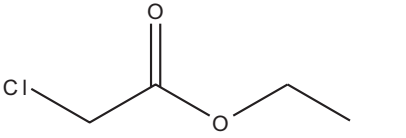
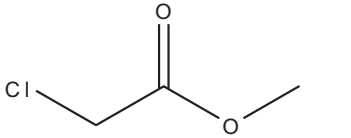
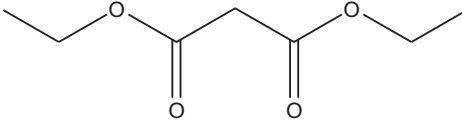
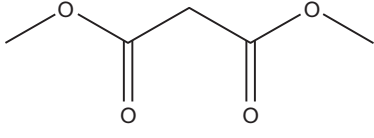
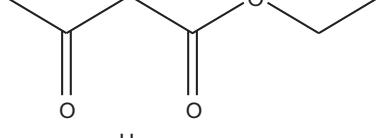
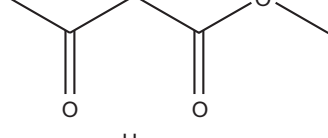
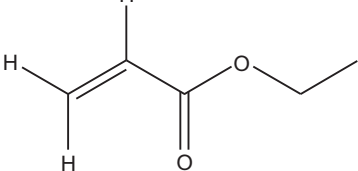
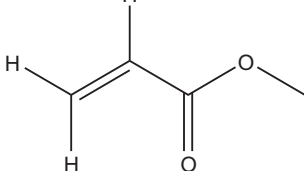


**Scheme 1.** General scheme for transesterification reaction.

### 3.6. Spectroscopic analysis

FT IR spectroscopy is a sensitive analytical tool for studying the structural details of the framework of silica based mesoporous materials. FT IR spectra of template containing (ZS-5A) and

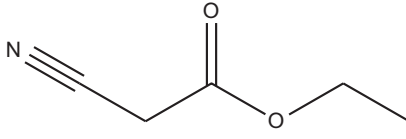
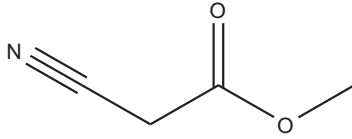
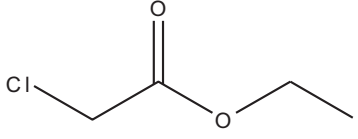
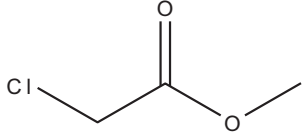
**Table 2**  
Transesterification of different esters with excess MeOH over ZS-5.

Entry	Substrate	Product	Conversion (%) <sup>a</sup>
1.			94.0
2.			46.2
3.			38.3
4.			25.2
5.			48.4

Conversion (%) = [Peak area of product obtained from GC / Summation of peak area of substrate and product obtained from GC] \* 100.

<sup>a</sup> Reaction condition: molar ratio of ester/MeOH = 1/250, catalyst = 0.05 g, temp. = 333 K, time = 24 h.

**Table 3**  
Transesterification of esters with MeOH using ZS-5 under solvent-free condition.

Entry	Substrate	Product	Conversion (%) <sup>a</sup>
1.			46.2
2.			3.0

Conversion (%) = [Peak area of product obtained from GC / Summation of peak area of substrate and product obtained from GC] \* 100.

<sup>a</sup> Reaction conditions: Ester: MeOH = 1:6, catalyst = 0.05 g, temperature = 333 K, time = 24 h.

template-free (ZS-5) Zn-doped mesoporous silica samples are shown in Fig. 10A and B, respectively. The broad peaks near 3400 and 1635  $\text{cm}^{-1}$  in both samples could be attributed to the adsorbed water molecules. Peaks at ca. 2850 and 2930  $\text{cm}^{-1}$  in ZS-5A, characteristics of C–H vibrations are not present in the calcined sample ZS-5, suggesting that it is totally free from template or any organic molecules. Peaks at ca. 792 and 1084  $\text{cm}^{-1}$  are attributed to the different characteristic Si–O–Si vibrations and defect Si–O–H stretching vibrations. Further, less intense peaks near ca. 950 and 569  $\text{cm}^{-1}$  could be assigned to the Zn–O–Si bonding and those at ca. 900, 585, 793  $\text{cm}^{-1}$  are characteristic of  $\text{Zn}_2\text{SiO}_4$  framework vibrations [32]. Absence of peak near 430  $\text{cm}^{-1}$  in both samples indicates the absence of ZnO clusters in this Zn-doped mesoporous silica sample [33]. The UV–visible spectroscopy is a very important technique to understand the coordination state of metal ions present in a given

matrix. Fig. 11 illustrates the UV–visible diffuse reflectance spectrum of template-free mesoporous ZS-5 sample. Two absorption bands near 256 and 300 nm together with very long tail are observed in the spectrum. The direct band gap estimated for the absorption band of this sample is 2.25 eV (inset of Fig. 11). This band gap energy is considerably lower than ZnO based nanostructure materials ( $E_g=3.3$  eV) [6]. Thus this mesoporous Zn-doped silica could have application in optoelectronics also.

#### 4. Transesterification reaction

Scheme 1 depicts the transesterification reaction of ester in presence of alcohol. We have explored the transesterification reaction over various mesoporous Zn-doped samples. We initiated the study with different mono- and di-ethyl esters, which are converted to their corresponding methyl esters in presence of excess MeOH present as esterifying agent at moderate temperature. The conversion of the reactants after 24 h reaction time is listed in Table 2. For the strong electro negativity of –CN group conversion % is quite high for the cyanoacetate ester in comparison to the other esters. No other solvent is used in this case since excess MeOH plays the role and also helps to shift the reaction equilibrium towards the desired product side. This fact is better observed when we use MeOH as a reagent to react with the ester (Table 3). The conversion has been reduced significantly, although same amount of catalyst and same reaction time was employed. ZS-10 and ZS-25 samples provide a lower conversion than ZS-5, although they have a close range of surface areas. This implies that zinc loading plays a crucial role in this reaction. The reacting ester can be activated by enhancing the electrophilicity of carbonyl carbon through coordination with vacant Lewis acidic site of zinc(II) [34]. Thus a higher percentage of Zn in ZS-5 promotes the product methyl ester in almost 94% yield. The conversions of methyl cyanoacetate ester in presence of excess

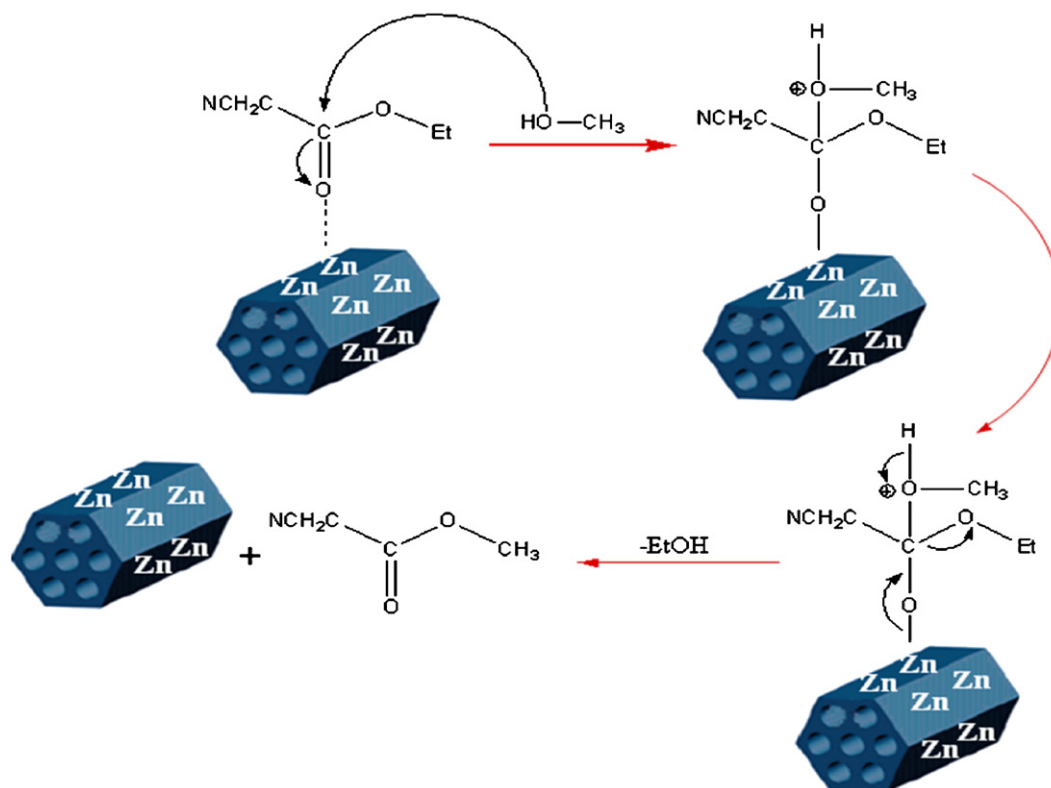
**Table 4**  
Comparison of the catalytic efficiency of all zinc doped mesoporous silica samples<sup>a</sup>.

Sample name	Zn % in the sample (AAS)	Substrate	Time (h)	Conversion (%) <sup>b</sup>
ZS-5	12.2	Ethyl cyanoacetate	24	94.0
ZS-10	10.9	Ethyl cyanoacetate	30	59.2
ZS-25	7.3	Ethyl cyanoacetate	30	47.4
$\text{SiO}_2^c$	0	Ethyl cyanoacetate	24	2.7

<sup>a</sup> Reaction conditions: Ester=1 mmol, MeOH=10 ml, ester: MeOH=1:250, catalyst=0.05 g, temperature=333 K.

<sup>b</sup> Conversion (%)=[Peak area of product obtained from GC/Summation of peak area of substrate and product obtained from GC]\*100.

<sup>c</sup> Zn-free mesoporous silica synthesized with CTAB/SDS.



**Scheme 2.** Schematic representation of the mechanism of transesterification of ethyl cyanoacetate over ZS sample.

**Table 5**  
Solvent effect in the transesterification of ethyl cyanoacetate with MeOH over ZS-5.

Entry	Solvent	Alcohol	Temperature (K)	Conversion (%) <sup>a</sup>
1.	Toluene	MeOH	333	10.0
2.	Acetonitrile	MeOH	333	-
3.	Chlorobenzene	MeOH	333	2.1
4.	Toluene	PhCH <sub>2</sub> OH	353	35.2
5.	Chlorobenzene	PhCH <sub>2</sub> OH	358	6.1
6.	Acetonitrile	PhCH <sub>2</sub> OH	338	16.2
7.	DMF	PhCH <sub>2</sub> OH	363	82.4
8.	DMF	1-BuOH	358	54.0
9.	DMF	2-PrOH	348	38.2

Conversion (%) = [Peak area of product obtained from GC/Summation of peak area of substrate and product obtained from GC] × 100.

<sup>a</sup> Reaction conditions: ethyl cyanoacetate = 10 mmol, alcohol = 20 mmol, solvent = 35 mmol, reaction time = 24 h, catalyst = 0.1 g.

MeOH over three mesoporous Zn-loaded silica samples are given in Table 4. When the reaction was carried out on 2D-hexagonal mesoporous silica devoid of any loaded Zn, almost no reaction occurred, suggesting the catalytic role played by the active Zn centers in this transesterification reaction. For convenience a suitable mechanism of transesterification reaction has been suggested in Scheme 2. The carbonyl oxygen atom coordinates to the Lewis acid site Zn center of ZS sample and electron deficiency generated on carbon atom is full filled by the oxygen of MeOH. A tetrahedral intermediate is formed from which EtOH molecule is released and the product methyl ester is obtained with regeneration of the catalyst.

The solvent effect on the transesterification of ethyl cyanoacetate has been studied using a variety of polar and non-polar solvents and the results are listed in Table 5. From the table it is clear that the reaction proceeds more successfully in polar solvent. This could be due to the fact that the products have good solubility in polar solvents. The change of the esterifying reagent, the alcohols also affects the yield of the reaction. This is because long chain aliphatic alcohols offer steric hindrance to the reaction site [35] and lead to lower yield of the product, although the reaction temperature is almost identical. Further, from this table (Table 5) it is seen that higher reactant conversion is obtained while changing the alcohol from aliphatic to aromatic (PhCH<sub>2</sub>OH). This could be attributed to the higher reactivity of the benzyl alcohol [36].

## 5. Conclusions

Mixture of cationic (CTAB) and anionic (SDS) surfactants along with metal-complexing agent tartaric acid have been found to be exceptionally efficient and unique for the synthesis of mesoporous 2D hexagonal zinc-doped silica material in aqueous medium under hydrothermal condition. Small angle XRD pattern of template-free sample shows long range ordering, while high temperature treatment converts the amorphous material to crystalline material having resemblance with Zn<sub>2</sub>SiO<sub>4</sub> structure. Presence of Zn in the silica framework has been verified from AAS and EDS analysis. Further, FT IR and UV-visible spectral studies prove successful incorporation of the zinc metal. BET surface area of Zn-doped silica

sample is appreciably high and pore diameter estimated using NLDFT method shows narrow distribution with maxima near 3.0 nm. Due to high Zn-loading in our mesoporous silica materials it could gain surface acidic property. Thus these materials efficiently catalyze the transesterification reaction under mild liquid-phase conditions.

## Acknowledgments

NP and MP are grateful to Council of Scientific and Industrial Research (CSIR), New Delhi for their senior research fellowships.

## References

- [1] S. Shimada, H. Otani, A. Miura, T. Sekiguchi, M. Yokoyama, J. Cryst. Growth 312 (2010) 452–456.
- [2] L. Fabbri, M. Licchelli, G. Rabaioli, A. Taglietti, Coord. Chem. Rev. 205 (2000) 85–108.
- [3] J.-M. Nedelec, L. Courtheoux, E. Jallot, C. Kinowski, J. Lao, P. Laquerriere, C. Mansuy, G. Renaudin, S. Turrell, J. Sol-Gel Sci. Technol. 46 (2008) 259–271.
- [4] J. Silvestre-Albero, J.C. Serrano-Ruiz, A. Sepulveda-Escribano, F. Rodriguez-Reinoso, Appl. Catal. A: Gen. 351 (2008) 16–23.
- [5] T. Hirai, M. Namba, I. Komasa, J. Colloid Interface Sci. 268 (2003) 394–399.
- [6] D. Chandra, S. Mridha, D. Basak, A. Bhaumik, Chem. Commun. (2009) 2384–2386.
- [7] G.S. Heo, I.G. Gim, J.W. Park, K.Y. Kim, T.W. Kim, J. Solid State Chem. 182 (2009) 2937–2940.
- [8] C. Soci, A. Zhang, B. Xiang, S.A. Dayeh, D.P.R. Aplin, X.Y. Bao, Y.H. Lo, D. Wang, Nano Lett. 7 (2007) 1003–1009.
- [9] M. Turco, G. Bagnasco, U. Costantino, F. Marmottini, T. Montanari, G. Ramis, G. Busca, J. Catal. 228 (2004) 43–55.
- [10] F. Ammari, J. Lamotte, R. Touroude, J. Catal. 221 (2004) 32–42.
- [11] Z. Yang, W. Xie, Fuel Process. Technol. 88 (2007) 631–638.
- [12] M.D. Serio, M. Ledda, M. Cozzolino, G. Minutillo, R. Tesser, E. Santacesaria, Ind. Eng. Chem. Res. 45 (2006) 3009–3014.
- [13] M. Alonso, F. Vila, R. Mariscal, M. Ojeda, M.L. Granados, J. Santamaria-Gonzalez, Catal. Today 158 (2010) 114–120.
- [14] T. Iwasaki, Y. Maegawa, Y. Hayashi, T. Ohshima, K. Mashima, J. Org. Chem. 73 (2008) 5147–5150.
- [15] C.T. Kresge, M.E. Leonowicz, W.J. Roth, J.C. Vartuli, J.S. Beck, Nature 359 (1992) 710–712.
- [16] G.S. Armatas, M.G. Kanatzidis, Nat. Mater. 8 (2009) 217–222.
- [17] S. Velu, L. Wang, M. Okasaki, K. Suzuki, S. Tomura, Micropor. Mesopor. Mater. 54 (2002) 113–126.
- [18] S.K. Das, M.K. Bhunia, A. Bhaumik, J. Solid State Chem. 183 (2010) 1326–1333.
- [19] M. Selvaraj, A. Pandurangan, K.S. Seshadri, P.K. Sinha, K.B. Lal, Appl. Catal. A: Gen. 242 (2003) 347–364.
- [20] R. Kumar, P. Mukherjee, A. Bhaumik, Catal. Today 49 (1999) 185–191.
- [21] S. Samanta, N.K. Mal, A. Bhaumik, J. Mol. Catal. A. Chem. 236 (2005) 7–11.
- [22] D. Zhao, A. Rodriguez, N.M. Dimitrijevic, T. Rajh, R.T. Koodali, J. Phys. Chem. C 114 (2010) 15728–15734.
- [23] D. Chandra, N.K. Mal, M. Mukherjee, A. Bhaumik, J. Solid State Chem. 179 (2006) 1802–1807.
- [24] D. Chandra, A. Bhaumik, Ind. Eng. Chem. Res. 45 (2006) 4879–4883.
- [25] T. Justel, H. Nikol, Adv. Mater. 12 (2000) 527–530.
- [26] A. Roy, S. Polarz, S. Rabe, B. Rellinghaus, H. Záhres, F.E. Kruijs, M. Driess, Chem. Eur. J. 10 (2004) 1565–1575.
- [27] S. Inagaki, Y. Fukushima, K. Kuroda, J. Chem. Soc. Chem. Commun. 8 (1993) 680–682.
- [28] P.T. Tanev, M. Chibwe, T.J. Pinnavaia, Nature 368 (1994) 321–323.
- [29] J. Xu, E.S. O'Keefe, C.C. Perry, J. Mater. Chem. 14 (2004) 1744–1748.
- [30] A.L. Patterson, Phys. Rev. 56 (1939) 978–982.
- [31] P.I. Ravikovitch, A. Neimark, J. Phys. Chem. B 105 (2001) 6817.
- [32] J.G. Ma, Y.C. Liu, C.S. Xu, Y.X. Liu, C.L. Shao, H.Y. Xu, J.Y. Zhang, Y.M. Lu, D.Z. Shen, X.E. Fan, J. Appl. Phys. 97 (2005) 103509.
- [33] S. Tural, Turk. J. Chem. 32 (2008) 169–179.
- [34] T. Kopke, M. Pink, J.M. Zaleski, Synlett 14 (2006) 2183–2186.
- [35] Y.H. Wang, Y.T. Gan, R. Whiting, G.Z. Lu, J. Solid State Chem. 182 (2009) 2530–2534.
- [36] N. Pal, M. Paul, A. Bhaumik, Appl. Catal. A: Gen. 393 (2011) 153–160.